NANO · MICRO small
www.small-journal.com

Multishelled Hollow Structures of Yttrium Oxide for the Highly Selective and Ultrasensitive Detection of Methanol

*Jianzhong Zheng, Tingmei Zhang, Huajie Zeng, Wei Guo, Bo Zhao, Yinghui Sun, Youyong Li, and Lin Jiang**

Methanol is extremely harmful to human health, since it is oxidized slowly and can accumulate in the human body. Therefore, it is essential to develop a methanol gas sensing technology with high sensitivity and selectivity for use in environmental monitoring and healthcare. In this work, a simple and low-cost sensor based on a Y_2O_3 multishelled hollow structure (YMSH) to selectively detect methanol with an ultrasensitive limit of detection (71 ppb) is developed. The unique multishelled hollow structure with a large surface area and exposed {222} facets makes an important contribution to the ultrasensitive detection of methanol, which is further confirmed by subsequent theoretical simulations. Moreover, in situ Fourier transform infrared spectra verify that CO_2 is the final product, which indicates a high catalytic activity of the YMSHs toward methanol oxidation. Interestingly, the sensor can also be applied to liquor samples that are mixtures of ethanol, methanol, and water, which provides a facile way to detect methanol in wines. This sensor represents a unique and highly sensitive means to detect methanol, which has great promise for potential application in environmental monitoring and food safety inspection.

1. Introduction

The energy crisis has become one of the most important problems facing the world today.[1–3] To meet increasing energy and environmental demands, methanol fuel cells are considered to be one of the best choices for clean and efficient power generation.[4–6] As the simplest alcohol, methanol is the most promising fuel additive candidate for internal combustion engines since it is inexpensive and easily handled, transported, and stored.[7–9] Moreover, methanol is present in the atmosphere,[10] deep-subsurface environments,[11] and even in interstellar space,[12] which makes it one of the most abundant compounds and the most prevalent of the gases.[13] However, experimentally detecting trace amounts of methanol around high-mass protostellar disks is largely unsuccessful.[13,14] Additionally, methanol is extremely harmful to human health because it paralyzes the central nervous system and damages the optic nerve and retina, causing blindness and death.[15,16] According to experimental results on animals, staying in a 35 ppm methanol steam for 30–60 min is dangerous for people. Worse still, methanol is different from other alcohols, since it is oxidized slowly and can accumulate in the human body. Hence, it is essential to detect methanol with high sensitivity and selectivity for environmental monitoring and healthcare purposes.

3D hierarchical-structured metal oxides have drawn wide attention in gas-sensing technology research in recent years due to their high surface area and abundance of accessible active sites, which can not only efficiently enhance molecular gas diffusion but also provide a number of active sites for enhancing the selectivity and catalytic activity.[17–25] To date, various 3D hierarchical-structured metal oxides with desirable morphologies and structures have been designed and synthesized to improve the performance of gas sensors, such as ZnO,[26–28] Co_3O_4,[29–31] SnO_2,[32,33] WO_3,[34–36] and In_2O_3.[37–39] Meanwhile, the exposed crystals of 3D hierarchical-structured metal oxides have also had a pivotal effect on the sensitivity and selectivity of gas sensors.[40–42] A number of methods based on 3D hierarchical structures, such as diode,[43] fluorescence,[44] luminescence,[45] and ellipsoidal nanospheres,[46] have been employed for methanol detection. However, methanol sensors based on electrical resistance can achieve a detection limit of 5 ppm, but the selectivity of detection is always too low to meet the requirements of practical applications.[46] Therefore, detection of methanol with both high sensitivity and selectivity remains a significant challenge. Moreover, wines unavoidably contain low concentrations of methanol, a reliable methanol sensor for selectively detecting methanol in mixed methanol and ethanol solutions is lacking as well. Among the oxide materials, yttrium oxide (Y_2O_3) with rare earth elements is one of the most attractive candidates for use in methanol sensors because of its excellent adsorption selectivity and high thermal and chemical stabilities.[47–52] However, thus far, desirable 3D hierarchical-structured yttrium oxide-based methanol gas sensors have never been proposed.

Herein, we have designed and fabricated a sensor based on a 3D hierarchical yttrium oxide multishelled hollow structure

Dr. J. Zheng, T. Zhang, H. Zeng, W. Guo, B. Zhao, Prof. Y. Sun, Prof. Y. Li, Prof. L. Jiang
Jiangsu Key Laboratory for Carbon-Based Functional Materials and Devices
Institute of Functional Nano and Soft Materials (FUNSOM)
Soochow University
Suzhou 215123, Jiangsu, P. R. China
E-mail: ljiang@suda.edu.cn

DOI: 10.1002/smll.201804688

(YMSHs) to detect methanol with high selectivity and an ultrasensitive limit (71 ppb). The cataluminescence (CTL) method is used for rapid identification of methanol, which provides a stable response using simple low-cost devices. The multishelled structure and the internal void space of 3D hierarchical yttrium oxide result in a larger surface area and more active sites than those of normal solid structures, which make important contributions to the ultrasensitive detection of methanol. Both experimental and simulation results confirm that the abundant {222} facets of the yttrium oxide multishelled hollow structures play a key role in the highly selective detection of methanol. Moreover, to identify the mechanism of the YMSH-dependent methanol CTL reaction, the final products of the reaction of methanol on the surface of the YMSHs were monitored by in situ Fourier transform infrared (FTIR) characterization techniques. Interestingly, this sensor can also be applied to liquor samples that are a mixture of ethanol, methanol, and water, which provides a facile way to detect methanol in wines. This sensor represents a unique and highly sensitive method to detect methanol, which has great promise for potential application in environmental monitoring and food safety inspection.

2. Results and Discussion

We designed a one-step hydrothermal method to produce carbon microspheres containing yttrium (Y^{3+}) ions and then obtained the 3D hierarchical yttrium oxide multishelled hollow structures through calcination, as shown in **Figure 1**a. Uniform carbon microspheres containing Y^{3+} ions with a diameter of ≈2.0 µm were prepared from a mixed solution including urea, yttrium chloride, and glucose using hydrothermal methods (Figure S1a, Supporting Information). An obvious diffraction peak in the X-ray powder diffraction (XRD) pattern was observed at ≈18° (Figure S1b, Supporting Information), which is characteristic of an amorphous carbon matrix. Meanwhile, the elemental mapping results of the carbon microspheres show that the elements of C, N, O, and Y were homogeneously distributed throughout the microspheres (Figure S1c,d, Supporting Information). The desirable highly crystalline yttrium oxide spheres with hierarchical multishelled hollow structures were constructed after annealing the carbon microspheres at 550 °C in air. As shown in Figure 1b, the XRD pattern of the yttrium oxide multishelled hollow structures revealed that this material

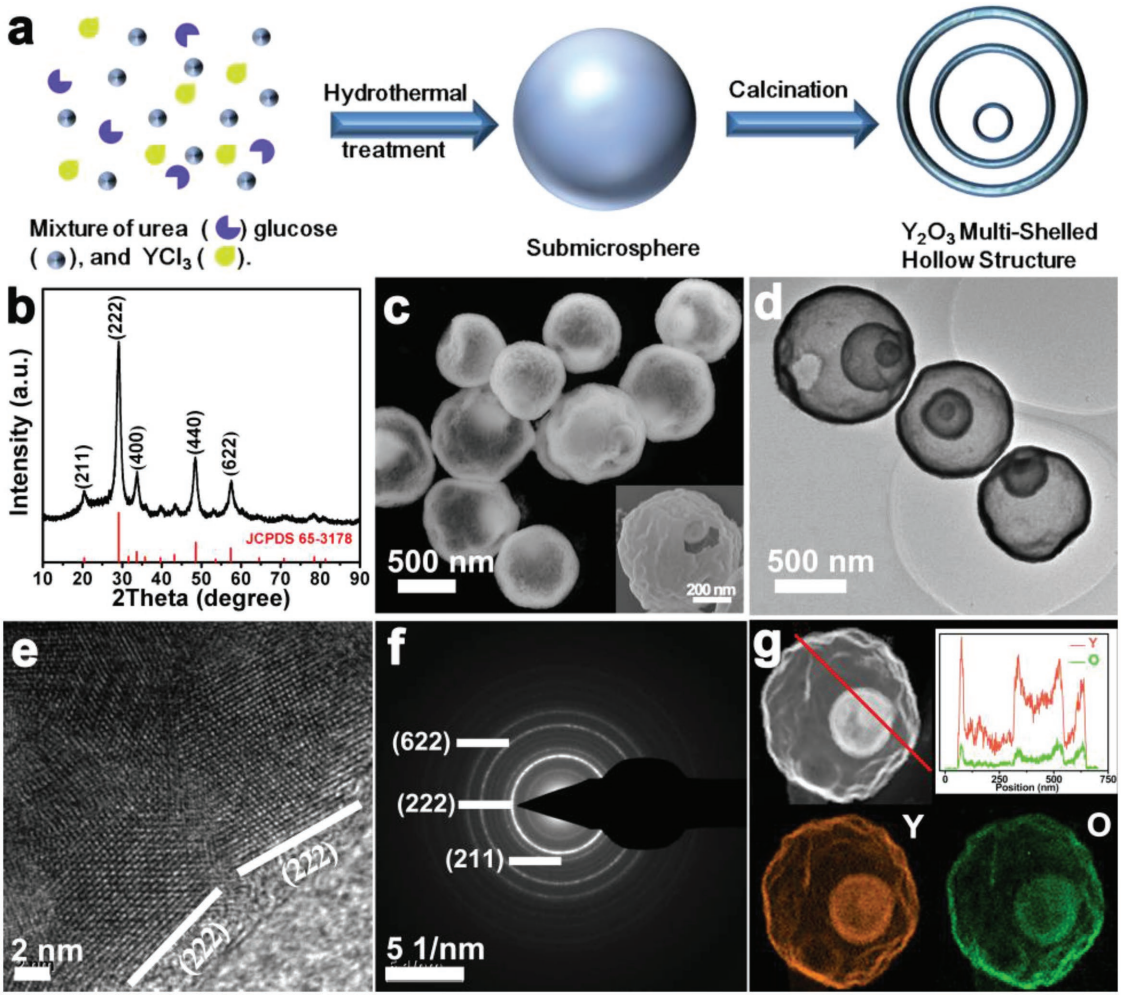

Figure 1. a) Scheme for the formation process of the yttrium-oxide multishelled hollow structure, b) XRD diffraction pattern, c) SEM image, d) TEM image, e) HRTEM image, f) SAED pattern, and g) HAADF-STEM image with the elemental mapping images and line scanning image of the YMSHs.

is in the cubic Y_2O_3 phase (JCPDS Card No. 65-3178). Additionally, an obvious (222)-plane peak was observed, which verifies the abundance of {222} crystal facets in the YMSHs. Scanning electron microscopy (SEM) images (Figure 1c) show that the multishelled hollow structures have a sharp contrast between the shells and hollow interiors, and their sizes are uniform with an average diameter of ≈900 nm. The multishelled hollow structures are further illustrated by the transmission electron microscopy (TEM) image (Figure 1d). The high-resolution TEM image (Figure 1e) reveals that exposed surfaces of the hollow spheres are primarily the {222} plane with a *d*-spacing of 0.307 nm, which agrees well with the XRD pattern. The diffraction rings of the selected area electron diffraction (SAED) indicate the polycrystalline characteristics of the material, which was further in agreement with the XRD results (Figure 1f). The hollow structures of the hierarchical multishelled yttrium-oxide material are further studied by high-angle annular dark-field scanning transmission electron microscopy (HAADFSTEM) mapping, as presented in Figure 1g, indicating that the multishelled yttrium-oxide structures are uniform and hollow, which is consistent with the above results. The formation of multishelled hollow spherical structures was further investigated by adjusting the quantities of $YCl_3 \cdot 6H_2O$, urea, and glucose in the reaction (Figures S2 and S3, Supporting Information). Multishelled hollow spherical structures were first obtained at 0.12 M glucose, as the mass of glucose increased from 0 to 0.18 M in the mixed solution with urea and YCl_3 (Figure S2, Supporting Information). It has been reported that monodisperse carbon microspheres can be prepared from glucose solutions by the hydrothermal method. After absorbing metal ions, the carbon microspheres act as sacrificial templates to generate metal oxide multishelled hollow structures after annealing at 550 °C in air.[53–56] Here, we used a one-step hydrothermal method to produce carbon microspheres containing yttrium (Y^{3+}) ions by introducing urea as a competing coordination agent. Without urea, the coordination of the Y^{3+} ions with glucose inhibits the formation of the carbon microspheres and multishelled structures cannot be generated (Figure S3, Supporting Information). The introduced urea exhibits a stronger coordination with the Y^{3+} ions compared to that of glucose, which results in the formation of carbon microspheres and the resultant multishelled hollow structures. Therefore, urea plays a crucial role in fabricating materials with multishelled structural morphologies by one-step hydrothermal treatment.

The morphological evolution of these YMSHs was intensively investigated as follows. From the thermogravimetric analysis (TGA) curve (Figure S4, Supporting Information), starting at 100 °C (I), the curves show a slight decline, which is due to the evaporation of water. From 200 to 550 °C (II), the curve presents a linear decline, which is attributed to the thermal decomposition of organics and combustion of the carbon components, during which the material loses 84% of its mass. After reaching 550 °C, the curve is flat, indicating that steady-state YMSHs were obtained. A TEM was employed to monitor the morphological evolution of the pre-YMSH materials during the annealing process, and the entire formation process is illustrated in **Figure 2**a. The pre-YMSH materials with highly smooth surfaces are shown in Figure 2b. Meanwhile, X-ray photoelectron spectroscopy (XPS) measurements were also conducted to explore the composition of the pre-YMSH materials, as illustrated in Figure S5a–c (Supporting Information). The peaks of the C 1s region are shown in Figure S5a (Supporting Information), and those at 284.5, 285.2, 286.3, and 288 eV are attributed to the C—C, C—N, C—O, and C=O bonds, respectively. The O—H bond (533.3 eV), C—O bond (532.5 eV), and C=O bond (531.3 eV) can be observed in the characteristic peaks of the O 1s region (Figure S5b, Supporting Information). The two kinds of Y 3d peaks, located at 158.5 and 156.4 eV, correspond to Y 3d3/2 and 3d5/2 of Y_2O_3, respectively, and a secondary doublet peak located at 160.3 and 158.3 eV was found in the Y 3d region (Figure S5d, Supporting Information), which

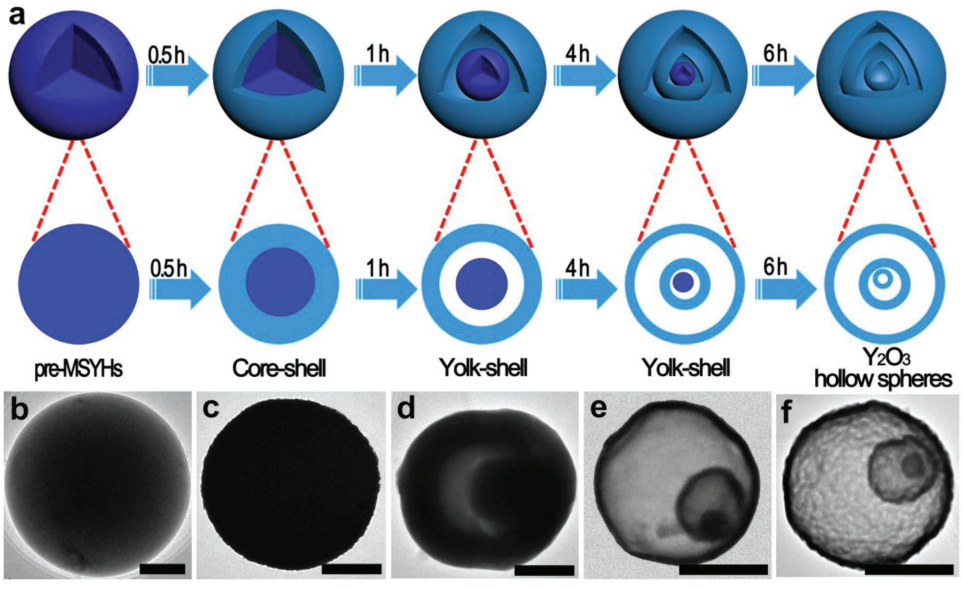

Figure 2. a) Schematic illustration of the formation mechanism of the YMSHs. b–f) TEM images of pre-YMSHs and the obtained product by annealing at 550 °C for different durations: 0, 0.5, 1, 4, and 6 h. All scale bars are 500 nm.

is consistent with previous reports.[57] The composition of the pre-YMSH materials was further confirmed by FTIR spectroscopy. The results are shown in Figure S5d (Supporting Information). The stretching vibration at 1150 cm^{-1} in the region of 1300–1000 cm^{-1} corresponds to the —OH group, and the vibration bands at 1630 and 1650 cm^{-1} correspond to the C=C and C=O groups, respectively. The N—H asymmetric stretching at 3436 cm^{-1} was attributed to the N—H of urea. Hence, amorphous pre-YMSH solid spheres are formed from yttrium ions, urea, and glucose. The color of the obtained core–shell structured sample with rough surfaces changes from deeply brown to black after annealing at 550 °C for 0.5 h (Figure 2c). However, because the annealing time (0.5 h) is short, the core–shell structure is not apparent. The HAADF-STEM and elemental mapping images of the pre-YMSH solid spheres after annealing at 550 °C for 0.5 h illustrate that amounts of the C, N, and O elements on the surface of the pre-YMSH solid spheres are reduced and these elements form particles during the annealing process (Figure S6, Supporting Information). As the annealing step is extended to 1 h, yolk–shell structures with a pre-YMSH core and a Y_2O_3 shell are observed as an intermediate product, as seen in Figure 2d. When further extending the annealing process, an obvious yolk–shell structure with a small solid core and two well-defined shells is seen (Figure 2e). Figure 2f shows that homogeneous YMSHs, as a unique 3D hierarchical structure, was successfully obtained after further extending the reaction time to 6 h.

A YMSH-based CTL sensor was fabricated to detect the analytes. The luminescence signal is generated and emitted due to the relaxation of excited products from their electronic excited state to the ground state during the catalytic oxidation reaction of the analyte molecule on the surface of YMSHs.[58–62] As reported in the literature, the luminescent intensity and signal-to-noise ratio (S/N) of the CTL response are strongly dependent on the detection wavelength, operating temperature, and flow rate.[58–62] The sensor response to 18 ppm methanol was tested through a series of interference (bandpass) filters in the range 400–640 nm to obtain the optimal wavelength (Figure S7, Supporting Information). With increasing wavelength, both the intensity and S/N reached a maximum at 490 nm and then decreased. Thus, 490 nm was regarded as the optimal wavelength for the following experiments. The response of the sensor toward different operating temperatures and flow rates was also investigated, as shown in Figures S8 and S9 (Supporting Information). The optimal temperature and flow rate were 100 °C and 240 mL min^{-1}, respectively, for the detection of methanol in the subsequent studies. Under the selected conditions described above, the CTL response profile of methanol on the YMSHs is evaluated by the sensor response and recovery times for three different concentrations of methanol vapor. The CTL intensity increased as the concentration of methanol vapor increased, while the response and recovery times were less than 10 and 60 s, respectively (**Figure 3**a). Figure 3b shows the reproducibility of the responses of the CTL sensor toward

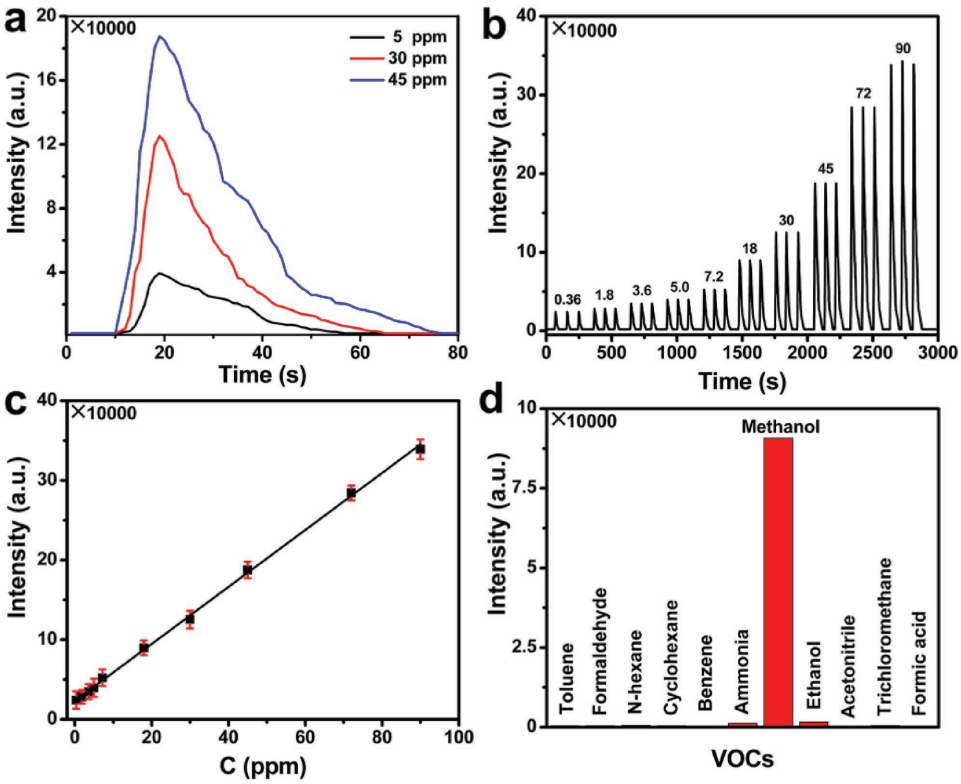

Figure 3. a) CTL spectra of the response and recovery times at different methanol concentrations, b) the reproducibility of the CTL response signals for methanol over a series of different concentrations ranging from 0.36 to 90 ppm, c) linear range of the calibration curves of the YMSHs, and d) the selectivity toward methanol of the methanol CTL gas sensor based on YMSHs. Conditions are wavelength: 490 nm, temperature: 100 °C, flow rate of the carrier gas: 240 mL min^{-1}.

methanol for a series of different concentrations ranging from 0.36 to 90 ppm. A linear calibration curve over the range of 0.36–90 ppm was obtained, and the linear regression equation is $I = 23119.67 + 3577.77\ C$, where the limit of detection is 71 ppb (S/N = 3), the correlation coefficient (R) is 0.9985, I is the average CTL intensity, and C is the concentration of methanol (Figure 3c). In addition, the CTL intensities at 18 ppm of methanol were recorded every 2 h over 7 d during the catalytic oxidation on the YMSHs. The results show no significant changes over time, which indicates a relatively long lifetime for the sensor (Figure S10, Supporting Information). Meanwhile, YMSHs were found to show an excellent selectivity toward methanol by investigating the sensor response to coexisting foreign substances, including formaldehyde, ethanol, benzene, *n*-hexane, formic acid, toluene, cyclohexane, trichloromethane, and ammonia, under the same concentrations and test conditions. As shown in Figure 3d, there is either no response or a weak response when a foreign volatile organic compound (VOC) is passed through the sensor.

To verify the impact of the 3D hierarchical structure of the YMSHs, commercially available solid Y_2O_3 nanoparticles (NPs) were used in a methanol CTL sensor for comparison, which was shown to exhibit poor sensitivity and selectivity for methanol detection under the same testing conditions (Figure S11, Supporting Information). Figure S12 (Supporting Information) shows the Brunauer–Emmett–Teller (BET) N_2 adsorption–desorption measurement results of the YMSHs and commercial Y_2O_3 nanoparticles. The YMSHs show a high specific surface area of 71.2 $m^2\ g^{-1}$ due to their unique multishelled structure, which is significantly higher than that of commercial Y_2O_3 nanoparticles at 6.3 $m^2\ g^{-1}$. The specific multishelled structures of the YMSHs offer a large active surface area that results in an enhancement of the CTL response because they exhibit more crystal facets that possess the desired active sites for the adsorption of methanol. Meanwhile, the porous hierarchical structures are favorable for the diffusion of the detected gas into/out of the sensor shells, which can also improve the response characteristics. Notably, the high-resolution TEM (HRTEM) image of the commercial solid Y_2O_3 NPs (Figure S13, Supporting Information) shows a mixture of exposed facets, including the {222}, {440}, and {400} facets. The XRD pattern results reveal that the ratio of the exposed {222} and {440} facets of the YMSHs is ≈1.8 times higher than that of the commercial Y_2O_3 NPs, which indicates that the {222} facet may directly correlate with the sensitivity and selectivity of the Y_2O_3 materials (Figure S14, Supporting Information). To confirm the above deduction, density functional theory (DFT) calculations were conducted to explore the methanol detection abilities of Y_2O_3, and all the detailed computational parameters can be found in the Supporting Information. We first studied the adsorption properties of methanol and the other coexisting foreign substances on the (222) plane of Y_2O_3, and the calculated adsorption configurations as well as the adsorption energies are shown in **Figure 4**. No obvious changes in molecular structure were observed after the methanol molecule or the other substances were adsorbed onto the Y_2O_3 substrate, and all the E_{ads} values were less than 1.5 eV. Therefore, it can be proven that all the substances can be physically adsorbed. The E_{ads} for methanol is the most negative, at −1.02 eV, among all the substances, which means that the {222} facets greatly benefit the adsorption of methanol and the subsequent catalysis compared with the benefits to the other substances. The similar adsorption energies for methanol and the other coexisting foreign substances on the (440) plane of Y_2O_3, by the DFT calculations, indicate that the {222} facet of Y_2O_3 presents a higher selectivity than does the {440} facet (Figure S15, Supporting Information), which can explain the high

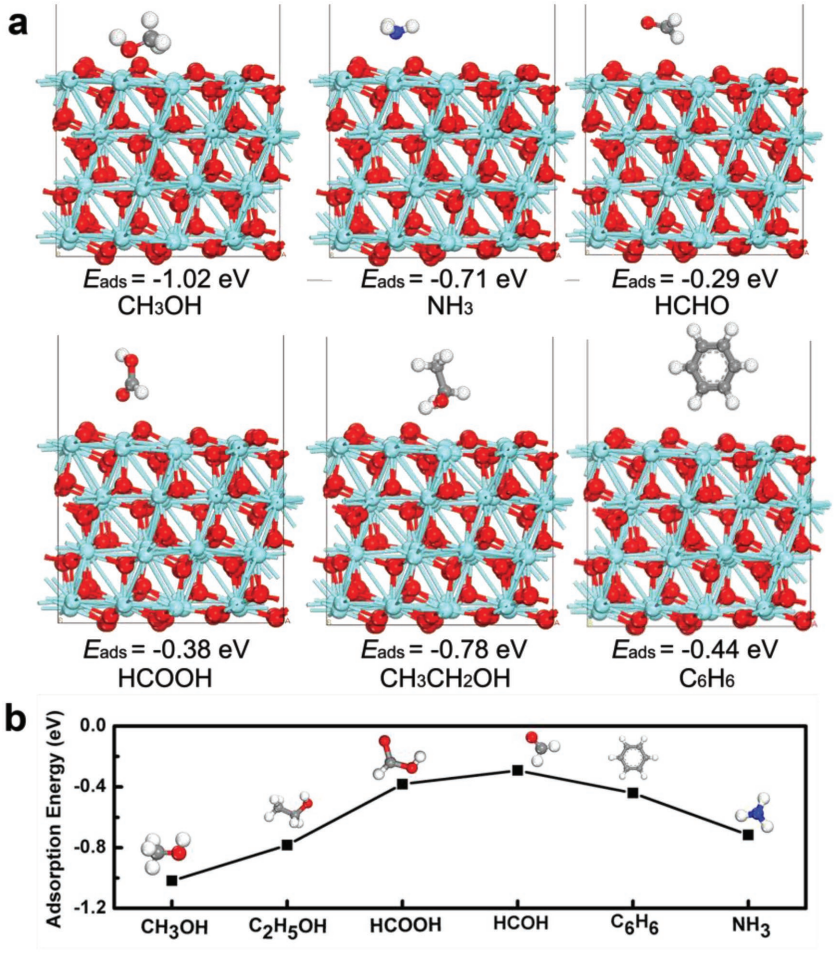

Figure 4. Theoretical simulation of the VOC adsorption ability of the YMSHs. a) Optimized adsorption structures of the geometric binding configurations and binding energies of the VOCs with the (222) plane of Y_2O_3. b) The adsorption energies and structures of different gasses on the Y_2O_3 surface. The gray, red, blue, and white balls denote C, O, N, and H atoms, respectively. A lower adsorption energy (further from zero) denotes a stronger adsorption.

methanol detection performance of the multishelled structures of Y_2O_3 compared with that of the commercial solid Y_2O_3 NPs. Moreover, single-shell Y_2O_3 hollow spheres were used in the methanol CTL sensor for comparison (Figure S16, Supporting Information), and they exhibited a lower relative CTL intensity than did the multishelled Y_2O_3 hollow spheres under the same testing conditions (Table S1, Supporting Information). Therefore, benefiting from the synergistic effects of a multishelled hollow structure with a large surface area and exposed {222} crystal facets, the sensor based on YMSHs shows a high selectivity and ultrasensitivity toward methanol, which is confirmed by the consistent experimental and simulated results.

The catalytic mechanism of methanol oxidation on the surface of the YMSHs was investigated to evaluate the correlation between the catalytic activity and CTL response. According to literature reports, there are many kinds of oxidative products from methanol, such as HCHO, CO, and CO_2.[63] The energy changes for the various oxidative products of methanol have been illustrated as follows

$$CH_3OH + 1/2O_2 \rightarrow H_2CO + H_2O \quad \Delta H = -159\ \text{kJ mol}^{-1} \tag{1}$$

$$CH_3OH + O_2 \rightarrow CO + 2H_2O \quad \Delta H = -389\ \text{kJ mol}^{-1} \tag{2}$$

$$CH_3OH + 3/2O_2 \rightarrow CO_2 + 2H_2O \quad \Delta H = -674\ \text{kJ mol}^{-1} \tag{3}$$

From the above chemical equations, it can be easily deduced that CO_2 is the final product of methanol oxidation since it has the maximum enthalpy change for the oxidation reaction. Here, the catalytic reaction final products of methanol on the surface of YMSHs were monitored by in situ FTIR characterization techniques. A new absorbance feature at 2350 cm^{-1} was observed after injecting 18 ppm of methanol, as seen in Figure S17 (Supporting Information), which is ascribed to the generation of CO_2 in the products. This result indicates that YMSHs demonstrate the highest catalytic activity for methanol oxidation, which further verifies the high methanol detection performance of these multishelled structures of Y_2O_3. A schematic illustration of the CTL configuration system for the identification of the methanol CTL reaction on the surface of the YMSHs is shown in **Figure 5**.

To further demonstrate the excellent selectivity of the YMSHs toward the detection of methanol, two groups of mixed gas (first group: 18 ppm methanol, 18 ppm ammonia, and 18 ppm formaldehyde; second group: 18 ppm methanol, 18 ppm ammonia, and 18 ppm benzene) were analyzed using the YMSH sensor (see Table S2, Supporting Information). According to the calibration curve of the CTL signal intensity versus concentration, 18.8 and 18.3 ppm of the analyte were detected, respectively. The relative standard deviation (RSD) of the CTL intensity is less than 3%, which represents a unique and high ability to distinguish methanol. Interestingly, our device is not only applicable to gas samples but is also suitable for liquid samples. It is well known that wines unavoidably contain low concentrations of methanol, and a reliable methanol sensor that can selectively detect methanol in mixed methanol and ethanol solutions is still in high demand. Herein, an aqueous mixture comprising 0.23 µL (18 ppm) of methanol, 6 mL of ethanol, and 4 mL of water was examined. A CaO tube was connected to the front end of the inlet of a quartz tube, which was used to remove water from the aqueous mixture during the detection test. Therefore, detection could proceed immediately after the removal of water. The analysis results show that there is 17.5 ppm of methanol in the mixture, which indicates these materials have great potential in the field of wine inspection.

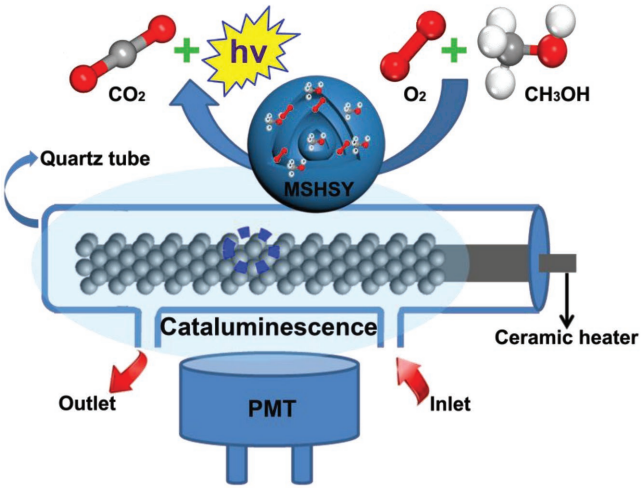

Figure 5. Schematic illustration of the configuration of the CTL system for the identification of methanol by the CTL reaction on YMSHs.

3. Conclusion

In conclusion, we have developed a simple and low-cost sensor based on 3D hierarchical Y_2O_3 multishelled hollow structures to detect methanol with high selectivity and ultrasensitivity (low limit of detection: 71 ppb). The unique hierarchical multishelled hollow structures have a large surface area and abundance of {222} facets, which contribute to the high selectivity and ultrasensitive detection of methanol and is confirmed by the consistent experimental and simulated results. The in situ FTIR spectral analysis results indicate that the YMSHs demonstrate the highest catalytic activity toward methanol oxidation, which further verifies the high methanol detection performance of the hierarchical multishelled Y_2O_3 structures. More interestingly, a sensor with a simple CaO apparatus can be applied to detect methanol in a liquid sample mixture of ethanol, methanol, and water, which represents a unique and strong ability to distinguish methanol. This simple method for detecting methanol can open the way to economical applications in environmental monitoring and food safety, including wine safety inspections.

4. Experimental Section

Synthesis of Yttrium Oxide Multishelled Hollow Structures: The YMSHs were prepared by a typical synthesis. A mixture of 6 mL of a 0.5 M urea solution and 6 mL of a 0.2×10^{-3} M $YCl_3 \cdot 6H_2O$ solution was slowly

added to 20 mL of 0.5 M glucose to form a homogeneous solution under vigorous stirring for 30 min. Then, the homogeneous solution was transferred to and sealed in a Teflon-lined autoclave and reacted at 160 °C for 24 h. Subsequently, after cooling to room temperature, the dark brown products were centrifuged and washed with additional deionized water several times before being placed in an oven to be dried at 60 °C for 12 h. Finally, the solid powder was calcined in a muffle furnace under air atmosphere at 550 °C for 360 min.

Sensor Fabrication: The CTL detection system was similar to that of a previous work.[64] Briefly, the present CTL sensor comprised three major parts: a laboratory-made reaction cell, a digital temperature controller (Chao Yang Automation Instrumentation Co., Ltd., Beijing, China), and a computerized BPCL ultraweak luminescent analyzer (Biophysics Institute of the Chinese Academy of Science, Beijing, China) equipped with a CR-105 photomultiplier tube (PMT, Model GDB23, Beijing Nuclear Instrument Factory, Beijing, China). The reaction cell was fabricated by placing a 4 mm diameter cylindrical ceramic heater (Ningbo Electric Iron Factory, Ningbo, China) in the middle of a 10 mL quartz tube equipped with a gas inlet and outlet. YMSH catalyst (0.4 g) was coated around the ceramic heater after the surface of the ceramic heater was brushed with glue (≈0.1 mL). The targeted temperature of the ceramic heater was controlled by a digital temperature controller, and then the ceramic heater with the YMSH catalyst was heated (500 °C, 3 h) to avoid the effects of previous absorbates at the beginning of the experiment. The CaO tube was arranged on the front end of the inlet of the quartz tube, which was used to remove water from the aqueous mixture during the detection test. Valve switches were installed at both the inlet and the outlet to allow the reaction cell to be opened (when the system was in the airstream flow reaction cell mode) or closed (when the system was in the closed reaction cell mode). A photomultiplier tube was used to detect and record the CTL signal produced by the catalytic reaction. The detection wavelengths were in the range of 400–640 nm, which could be selected for by changing the interference optical filters, which had a bandwidth of 24 nm (Institute of Biophysics, Academia Sinica, Beijing, China).

Computational Details: All spin-polarized DFT calculations were implemented in the Dmol^3 program.[65,66] The Perdew, Burke, and Ernzerhof (PBE) exchange-correlation functional within the generalized gradient approximation (GGA) was chosen for the calculations.[67] The van der Waals interactions were introduced into the calculations through a Grimme empirical dispersion correction scheme.[68] The density functional semicore pseudopotential (DSPP)[69] was selected to address the core electrons and the relativistic effects induced by heavier elements. The double-numerical atomic orbital plus polarization function (DNP) was taken into consideration to be the basis set. The convergence tolerance of the self-consistent field (SCF) was 1.0×10^{-6} Ha (1 Ha = 27.21 eV) for the geometry optimization and total electronic energy calculations.

A stoichiometric slab model of four O-Y-O layers was cleaved from the optimized bulk crystal structure in the (222) and (440) directions. The atom coordinate of the bottom two layers was held fixed while that of the uppermost two layers was allowed to relax to their equilibrium position during the geometry optimization process. A vacuum region of ≈20 Å was set to separate the periodic images. The Brillouin zone was sampled with $3 \times 3 \times 1$ k-points.

Adsorption energy (E_{ads}) was chosen to be the descriptor and was defined as $E_{ads} = E_{total} - E_{substrate} - E_{molecule}$, where E_{total} is the total energy of the different gas molecules adsorbed onto the Y_2O_3 substrate, $E_{substrate}$ and $E_{molecule}$ are the energies of the Y_2O_3 substrate and the isolated molecule, respectively; thus, a negative E_{ads} means an energetically stable configuration.

Supporting Information

Supporting Information is available from the Wiley Online Library or from the author.

Acknowledgements

This work was supported by National Key R&D Program of China (International Collaboration program) granted by Chinese Ministry of Science and Technology (2016YFE0129800) and the National Natural Science Foundation of China (21822202 and 21507054). This project was supported by the Special Scientific Research Fund of the National General Administration of Quality Supervision in China (2018IK027). This was also a project supported by the Natural Science Foundation of Jiangsu Province (BK20150007), project funded by 111 project, Joint International Research Laboratory of Carbon-Based Functional Materials and Devices, Collaborative Innovation Center of Suzhou Nano Science & Technology, and the Priority Academic Program Development of Jiangsu Higher Education Institutions (PAPD). The authors acknowledge Prof. Mingwang Shao for discussing the results about structure characterization.

Conflict of Interest

The authors declare no conflict of interest.

Keywords

cataluminescence, methanol, multishelled hollow structure, volatile organic compounds, yttrium oxide

Received: November 9, 2018
Revised: December 19, 2018
Published online:

[1] M. Li, Z. Zhao, T. Cheng, A. Fortunelli, C. Y. Chen, R. Yu, Q. Zhang, L. Gu, B. V. Merinov, Z. Lin, E. Zhu, T. Yu, Q. Jia, J. Guo, L. Zhang, W. A. Goddard III, Y. Huang, X. Duan, *Science* **2016**, *354*, 1414.
[2] J. M. Clomburg, A. M. Crumbley, R. Gonzalez, *Science* **2017**, *355*, aag0804.
[3] L. Liang, F. C. Lei, S. Gao, Y. F. Sun, X. C. Jiao, J. Wu, S. Qamar, Y. Xie, *Angew. Chem., Int. Ed.* **2015**, *54*, 13971.
[4] G. A. Olah, A. Goeppert, G. K. S. Prakash, *Methanol and Dimethyl Ether as Fuels and Energy Carriers*, Wiley-VCH, Weinheim, Germany **2009**.
[5] K. Sordakis, C. H. Tang, L. K. Vogt, H. Junge, P. J. Dyson, M. Beller, G. Laurenczy, *Chem. Rev.* **2018**, *118*, 372.
[6] S. Gao, B. C. Gu, X. C. Jiao, Y. F. Sun, X. L. Zu, F. Yang, W. G. Zhu, C. M. Wang, Z. M. Feng, B. J. Ye, Y. Xie, *J. Am. Chem. Soc.* **2017**, *139*, 3438.
[7] A. Álvarez, A. Bansode, A. Urakawa, A. V. Bavykina, T. A. Wezendonk, M. Makkee, J. Gascon, F. Kapteijn, *Chem. Rev.* **2017**, *117*, 9804.
[8] Z. Liu, Z. Yin, C. Cox, M. Bosman, X. Qian, N. Li, H. Zhao, Y. Du, J. Li, D. G. Nocera, *Sci. Adv.* **2016**, *2*, e1501425.
[9] M. Nielsen, E. Alberico, W. Baumann, H. J. Drexler, H. Junge, S. Gladiali, M. Beller, *Nature* **2013**, *495*, 85.
[10] L. G. Gao, J. J. Zheng, A. Fernandez-Ramos, D. G. Truhlar, X. J. Xu, *J. Am. Chem. Soc.* **2018**, *140*, 2906.
[11] D. Z. Sousa, M. Visser, A. H. Gelder, S. Boeren, M. M. Pieterse, M. W. H. Pinkse, P. D. Verhaert, C. Vogt, S. Franke, S. Kümmel, A. J. M. Stams, *Nat. Commun.* **2018**, *9*, 239.
[12] R. J. Shannon, M. A. Blitz, A. Goddard, D. E. Heard, *Nat. Chem.* **2013**, *5*, 745.
[13] B. Lankhaar, W. Vlemmings, G. Surcis, H. J. Langevelde, G. C. Groenenboom, V. Ad Avoird, *Nat. Astron.* **2018**, *2*, 145.
[14] C. K. Jen, *Phys. Rev.* **1951**, *81*, 197.

[15] A. J. Paine, A. D. Dayan, *Hum. Exp. Toxicol.* **2001**, *20*, 563.
[16] Q. Zhu, Y. M. Zhang, J. Zhang, Z. Q. Zhu, Q. J. Liu, *Sens. Actuators, B* **2015**, *207*, 398.
[17] J. Bai, B. X. Zhou, *Chem. Rev.* **2014**, *114*, 10131.
[18] T. Wagner, S. Haffer, C. Weinberger, D. Klaus, M. Tiemann, *Chem. Soc. Rev.* **2013**, *42*, 4036.
[19] A. K. Nayak, R. Ghosh, S. Santra, P. K. Guha, D. Pradhan, *Nanoscale* **2015**, *7*, 12460.
[20] Y. J. Bae, P. V. Pikhitsa, H. Cho, M. Choi, *Adv. Mater.* **2017**, *29*, 1604159.
[21] J. J. Zhang, P. G. Tang, T. Y. Liu, Y. J. Feng, C. Blackman, D. Q. Li, *J. Mater. Chem. A* **2017**, *5*, 10387.
[22] Y. M. Wang, Q. D. Chen, X. H. Shen, *Chin. Chem. Lett.* **2017**, *28*, 197.
[23] Y. T. Zuo, J. Peng, G. Li, L. Liu, Z. S. Han, G. Wang, *Chin. Chem. Lett.* **2016**, *27*, 887.
[24] L. Wan, H. Y. Song, J. H. Ma, Y. Ren, X. W. Cheng, J. C. Su, Q. Yue, Y. H. Deng, *ACS Appl. Mater. Interfaces* **2018**, *10*, 13028.
[25] X. Yang, X. W. Cheng, H. Y. Song, J. H. Ma, P. P. Pan, A. A. Elzatahry, J. C. Su, Y. H. Deng, *Adv. Healthcare Mater.* **2018**, *7*, 1800149.
[26] K. Hagedorn, W. Y. Li, Q. J. Liang, S. Dilger, M. Noebels, M. R. Wagner, J. S. Reparaz, A. Dollinger, J. S. Günne, T. Dekorsy, L. Schmidt-Mende, S. Polarz, *Adv. Funct. Mater.* **2016**, *26*, 3424.
[27] X. R. Zhou, Y. H. Zhu, W. Luo, Y. Ren, P. C. Xu, A. A. Elzatahry, X. W. Cheng, A. Alghamdi, Y. H. Deng, D. Y. Zhao, *J. Mater. Chem. A* **2016**, *4*, 15064.
[28] F. D. Qu, H. F. Jiang, M. H. Yang, *Nanoscale* **2016**, *8*, 16349.
[29] L. Li, M. M. Liu, S. J. He, W. Chen, *Anal. Chem.* **2014**, *86*, 7996.
[30] Y. Y. Lu, W. W. Zhan, Y. He, Y. T. Wang, X. J. Kong, Q. Kuang, Z. X. Xie, L. S. Zheng, *ACS Appl. Mater. Interfaces* **2014**, *6*, 4186.
[31] J. S. Jang, W. T. Koo, S. J. Choi, I. D. Kim, *J. Am. Chem. Soc.* **2017**, *139*, 11868.
[32] C. Marichy, N. Donato, M. G. Willinger, M. Latino, D. Karpinsky, S. H. Yu, G. Neri, N. Pinna, *Adv. Funct. Mater.* **2011**, *21*, 658.
[33] a) X. Xu, J. Zhuang, X. Wang, *J. Am. Chem. Soc.* **2008**, *130*, 12527; b) H. K. Wang, A. L. Rogach, *Chem. Mater.* **2014**, *26*, 123.
[34] Y. H. Li, W. Luo, N. Qin, J. P. Dong, J. Wei, W. Li, S. S. Feng, J. C. Chen, J. Q. Xu, A. A. Elzatahry, M. H. Es-Saheb, Y. H. Deng, D. Y. Zhao, *Angew. Chem., Int. Ed.* **2014**, *53*, 9035.
[35] Y. S. Zhu, Y. Zhao, J. H. Ma, X. W. Cheng, J. Xie, P. C. Xu, H. Q. Liu, H. P. Liu, H. J. Zhang, M. H. Wu, A. A. Elzatahry, A. Alghamdi, Y. H. Deng, D. Y. Zhao, *J. Am. Chem. Soc.* **2017**, *139*, 10365.
[36] J. H. Ma, Y. Ren, X. R. Zhou, L. L. Liu, Y. H. Zhu, X. W. Cheng, P. C. Xu, X. X. Li, Y. H. Deng, D. Y. Zhao, *Adv. Funct. Mater.* **2018**, *28*, 1705268.
[37] T. Waitz, T. Wagner, T. Sauerwald, C. Kohl, M. Tiemann, *Adv. Funct. Mater.* **2009**, *19*, 653.
[38] Y. Ren, X. R. Zhou, W. Luo, P. C. Xu, Y. H. Zhu, X. X. Li, X. W. Cheng, Y. H. Deng, D. Y. Zhao, *Chem. Mater.* **2016**, *28*, 7997.
[39] X. R. Zhou, X. W. Cheng, Y. H. Zhu, A. A. Elzatahry, A. Alghamdi, Y. H. Deng, D. Y. Zhao, *Chin. Chem. Lett.* **2018**, *29*, 405.
[40] M. D'Arienzo, D. Cristofori, R. Scotti, F. Morazzoni, *Chem. Mater.* **2013**, *25*, 3675.
[41] J. Jońca, A. Ryzhikov, M. L. Kahn, K. Fajerwerg, A. Chapelle, P. Menini, P. Fau, *Chem. - Eur. J.* **2016**, *22*, 10127.
[42] Z. Li, C. K. Dong, J. Yang, S. Z. Qiao, X. W. Du, *J. Mater. Chem. A* **2016**, *4*, 2699.
[43] T. Y. Tiong, C. F. Dee, A. A. Hamzah, B. Y. Majlis, S. A. Rahman, *Sens. Actuators, B* **2014**, *202*, 1322.
[44] J. Zhang, Y. Nosaka, *Appl. Catal., B* **2015**, *166*, 32.
[45] J. Wang, M. Jiang, L. Yan, R. Peng, M. J. Huangfu, X. X. Guo, Y. Li, P. Y. Wu, *Inorg. Chem.* **2016**, *55*, 12660.
[46] C. Wang, X. Y. Kou, N. Xie, L. L. Guo, Y. F. Sun, X. H. Chuai, J. Ma, P. Sun, Y. Wang, G. Y. Lu, *ACS Sens.* **2017**, *2*, 648.
[47] G. Wakefield, E. Holland, P. J. Dobson, J. L. Hutchison, *Adv. Mater.* **2001**, *13*, 1557.
[48] J. A. Nelson, E. L. Brant, M. J. Wagner, *Chem. Mater.* **2003**, *15*, 688.
[49] J. Guzman, A. Corma, *Chem. Commun.* **2005**, 743.
[50] Y. N. Xu, Z. Q. Gu, W. Y. Ching, *Phys. Rev. B* **1997**, *56*, 14993.
[51] N. Chen, L. Ji, G. P. Du, *J. Lumin.* **2014**, *153*, 259.
[52] R. C. Plaza, L. Zurita, J. D. G. Durán, F. González-Caballero, A. V. Delgado, *Langmuir* **1998**, *14*, 6850.
[53] J. Y. Wang, H. J. Tang, L. J. Zhang, H. Ren, R. B. Yu, Q. Jin, J. Qi, D. Mao, M. Yang, Y. Wang, P. R. Liu, Y. Zhang, Y. R. Wen, L. Gu, G. H. Ma, Z. G. Su, Z. Y. Tang, H. J. Zhao, D. Wang, *Nat. Energy* **2016**, *1*, 16050.
[54] X. Y. Lai, J. Li, B. A. Korgel, Z. H. Dong, Z. M. Li, F. B. Su, J. Du, D. Wang, *Angew. Chem., Int. Ed.* **2011**, *50*, 2738.
[55] J. Qi, X. Y. Lai, J. Y. Wang, H. J. Tang, H. Ren, Y. Yang, Q. Jin, L. J. Zhang, R. B. Yu, G. H. Ma, Z. G. Su, H. J. Zhao, D. Wang, *Chem. Soc. Rev.* **2015**, *44*, 6749.
[56] J. Y. Wang, H. J. Tang, H. Ren, R. B. Yu, J. Qi, D. Mao, H. J. Zhao, D. Wang, *Adv. Sci.* **2014**, *1*, 1400011.
[57] J. Kim, P. C. Shih, K. C. Tsao, Y. T. Pan, X. Yin, C. J. Sun, H. Yang, *J. Am. Chem. Soc.* **2017**, *139*, 12076.
[58] D. Liu, M. Y. Liu, G. H. Liu, S. C. Zhang, Y. Y. Wu, X. R. Zhang, *Anal. Chem.* **2010**, *82*, 66.
[59] M. R. Almasian, N. Na, F. Wen, S. C. Zhang, X. R. Zhang, *Anal. Chem.* **2010**, *82*, 3457.
[60] N. Na, S. C. Zhang, S. A. Wang, X. R. Zhang, *J. Am. Chem. Soc.* **2006**, *128*, 14420.
[61] J. Y. Han, F. F. Han, J. Ouyang, L. X. He, Y. T. Zhang, N. Na, *Nanoscale* **2014**, *6*, 3069.
[62] L. Q. Wu, L. C. Zhang, M. X. Sun, R. Liu, L. Z. Yu, Y. Lv, *Anal. Chem.* **2017**, *89*, 13666.
[63] M. Bowker, R. Holroyd, A. Elliott, P. Morrall, A. Alouche, C. Entwistle, A. Toerncrona, *Catal. Lett.* **2002**, *83*, 165.
[64] S. F. Li, J. Z. Zheng, W. X. Zhang, J. Cao, S. X. Li, Z. M. Rao, *Analyst* **2013**, *138*, 916.
[65] B. Delley, *J. Chem. Phys.* **1990**, *92*, 508.
[66] B. Delley, *J. Chem. Phys.* **2000**, *113*, 7756.
[67] J. P. Perdew, K. Burke, M. Ernzerhof, *Phys. Rev. Lett.* **1996**, *77*, 3865.
[68] S. Grimme, *J. Comput. Chem.* **2006**, *27*, 1787.
[69] B. Delley, *Phys. Rev. B* **2002**, *66*, 155125.